The Structural and Electrical Characteristics of Silicon-Implanted Borosilicate Glass

2002 Jpn. J. Appl. Phys. 41 L1379

(http://iopscience.iop.org/1347-4065/41/12A/L1379)

Jpn. J. Appl. Phys. Vol. 41 (2002) pp. L 1379–L 1382
Part 2, No. 12A, 1 December 2002

The Structural and Electrical Characteristics of Silicon-Implanted Borosilicate Glass

Gong-Ru LIN*

Institute of Electro-Optical Engineering, National Chiao Tung University, 1001 Ta Hsueh Rd., Hsinchu, Taiwan 300, R.O.C.

(Received May 29, 2002; revised manuscript received September 12, 2002; accepted for publication October 7, 2002)

The structural and electrical properties of silicon-implanted borosilicate glass (BSO:Si^+) are studied. The nearly amorphous phase of as-implanted BSO:Si^+ with a weak and broadened X-ray diffraction peak transforms into crystallite phases with associated peaks positioned at azimuth angles of 29° and 14° after thermal annealing. These peaks correspond to (111)-oriented Si nanocrystals of 0.6–0.8 nm size and the regrown (021)-oriented BSO host, respectively. The intensity of the photoluminescent (PL) peak of the BSO:Si^+ centered at 520 nm is found to decrease due to both the elimination of the radiative defects and the precipitation of Si nanocrystals, however, nanocrystal-related PL is not initiated even after low-temperature and long-term (> 4 h) annealing. Relatively high leakage current Schottky diodes with contact patterns for transmission line measurement (TLM) made on as-implanted BSO:Si^+ reveal the defect-enhanced current transport mechanism. After annealing at 500°C for 60 min or longer, the leakage current of the BSO:Si^+ diode dramatically decreases by at least two orders of magnitude. The current–voltage analysis attributes the disappearance of the resonant tunneling behavior of the TLM diode made on as-implanted BSO:Si^+ with negative differential resistance to the annealing-induced reduction of radiative defect concentration. [DOI: 10.1143/JJAP.41.L1379]

KEYWORDS: silicon, implanted, borosilicate glass, nanocrystal, defects, negative differential resistance

Nanocrystallite Si semiconductor structure has recently been investigated for its potential application to direct-bandgap optoelectronics. Previously, considerable interest was focused on the porous Si[1,2] and Si[3–7] ultrafine particles or nanocrystals due to their optical properties. Earlier reports on the strong room-temperature luminescence in nanocrystallite[5] and porous Si[8] have stimulated the development and application of such materials[9] in light-emitting devices.[10] Later, Si nanocrystals were synthesized in the SiO_2 matrices on silicon substrate via implantation and annealing processes.[11] Such materials exhibit strong photo- and electroluminescence (PL and EL) in visible and near-infrared wavelengths, which attracts much attention due to the potential applications in electronic and optoelectronic devices.[12–15] Most of the studies on these materials discuss light-emitting properties of the metal-oxide-semiconductor (MOS) structure with Si nanocrystals buried in the surface oxide layer on the silicon substrate. The combined carrier transport effects of the conventional MOS diode, the implanted Si-related defects, and the buried Si nanocrystals in the SiO_2 layer on Si substrate are thus complicated. In contrast, the electrical properties of the silicon nanocrystals embedded in the quartz or glass substrate, or the oxide film without semiconducting substrate are not frequently encountered. Borosilicate (BSO) glass was always employed as the host of Si nanocrystals in previous studies. The decreased PL intensity of the as-implanted or the annealed BSO:Si^+ with buried Si nanocrystals due to the existence of p-type Boron states was reported. For future study, the competition between implanted Si-related radiative defects and boron-related non-radiative recombination centers and the photo-excited carrier dynamics in the BSO:Si^+ samples are of great interest. In this article, we report the formation of nanocrystallite Si semiconductor by multi-energy implantation of silicon ions into BSO glass substrate. The optical and electrical properties of the BSO:Si^+ sample are characterized by using X-ray diffractometry (XRD), photoluminescence (PL), transmission line measurement (TLM), and current–voltage (I–V) analysis. The XRD and PL analysis provide important information on the evolution of radiative defect density and the precipitation of Si nanocrystals in BSO:Si^+ during annealing. The TLM and I–V characterizations of the Al-evaporated metal contacts made on the BSO:Si^+ substrate were used to investigate the resonant tunneling behavior of the as-implanted BSO:Si^+ with negative differential resistance, and the decreasing leakage current associated with reduced defect concentration of BSO:Si^+ which was long-term annealed at 500°C. Key parameters such as the defect-related PL wavelengths, the size and orientation of Si nanocrystals in BSO:Si^+, the leakage current, the contact resistance, and the sheet resistivity of the TLM Schottky diodes made on such material are also determined.

The BSO:Si^+ samples were prepared by implanting BSO glass with thickness of 125 ± 20 mm with 50, 100, and 200 keV silicon ions at the dosage of 10^{16} ions/cm^2. The depth of implantation is theoretically estimated to be up to 350 nm below the surface by using the Monte-Carlo simulation program. Optimized annealing of the BSO:Si^+ at 500°C for 30 min to obtain maximum PL signal was carried out according to the method of Rebohle *et al.*[16] In our experiment, the furnace-annealing process at 500°C ranging from 30 to 120 min at 30 min increments was employed to modify the carrier transport property of the BSO:Si^+ samples. The structural property of the deposited BSO:Si^+ was characterized by XRD measurements in the θ–2θ scanning mode with Cu-Kα radiation source ($\lambda = 1.5418$ Å). The spacing between the desired planes is calculated from Bragg's law $n\lambda = 2d \sin\theta$, where λ is the wavelength of Cu-Kα radiation, θ is the Bragg angle, and n is a positive integer. The PL spectra were taken at room temperature using a commercial fluorescence photospectrometer (Fluorolog ISO IOBINYUON-SPEX) with excitation wavelength of 270 nm. The 100-nm-thick aluminum-evaporated Schottky contact patterns for TLM analysis of the leakage current and the contact resistance of the BSO:Si^+ diode were fabricated with contact size of $75 \times 50\,\mu m^2$ and spacing ranging from 2.5 μm to 25 μm at 5 μm increment. After measuring the resistances of the BSO:Si^+ diodes with different gap spacings, the specific contact resistivity, lateral

*E-mail address: grlin@faculty.nctu.edu.tw

contact resistance, and sheet resistance can be evaluated from the relationship $R_i = 2R_c + R_s l_i/w$, where R_i is the measured resistance between the two contacts separated by l_i, R_c is the contact resistance, and R_s is the sheet resistance of the material. The plot of R_i as a function of l_i (with a slope of R_s/w) has an intercept of $-2R_c w/R_s$ at the x-axis and an intercept of $2R_c$ at the y-axis. The specific contact resistivity of the BSO:Si$^+$ ($\rho_c = \omega^2 R_c^2/R_s$) can thus be obtained from calculation of the experimental data.

It is found that the XRD diffraction peak of the as-implanted BSO:Si$^+$ has split after annealing, as shown in Fig. 1. The as-implanted BSO:Si$^+$ shows only a weak and broadened diffraction pattern due to presence of the silicon dioxide. After annealing, a relatively weak peak at $2\theta = 28$–$29°$ is formed due to the recrystalization of (111)-oriented Si matrices in the BSO:Si$^+$. The precipitation of Si nanocrystals is believed to be initiated during the long-term and low-temperature annealing process, however, the nanocrystals have sub-nm diameters unlike typical Si nanocrystals (> 1.6 nm) formed under high temperature condition. The measurement of the size and density of considerably smaller Si nanocrystals in the BSO:Si$^+$ thus relies on a high-resolution transmission electron microscopy. Nonetheless, the size can still be evaluated by using Scherre's relation,[17] size $= 0.9\lambda/(\beta \cos\theta)$ nm, where λ is the wavelength of the XRD source (0.15418 nm), β is the full-width at half maximum (FWHM) of the broadened XRD diffraction peak (in units of radian), and θ is the diffraction angle. In our BSO:Si$^+$, the FWHM of the (111)-oriented Si-related XRD peak is about 1.75–2.27×10^{-1} radian (10°–13°), which gives rise to (111)-oriented Si nanocrystals ranging from 0.63 to 0.82 nm in size. A relatively stronger diffraction peak located at $2\theta = 14°$ was also observed for the annealed BSO:Si$^+$ sample, which is similar to that of (021)-oriented solid crystalline SiO_2 phase according to the diffraction database.[18] In comparison, Sandhu *et al.*[17] previously studied the effect of annealing on silicon-doped SiO_2 film and reported relatively similar XRD diffraction peaks. The authors attributed the observed peak centered at $2\theta = 24°$ with FWHM of 7.5° to the Si-rich SiO_2 substrate. After annealing at 1100°C for 1 h, the original rocking-curve peak is split into two adjacent peaks and other sub-peaks centered at 20.5°, 28.5°, 47.3° and 56°. The former peak at 20.5° is also explained as the contribution of the SiO_2 matrices, and the latter three peaks are attributed to solid crystalline silicon phases (silicon crystallites) with orientations of (111), (220), and (311), respectively.

The PL spectra of as-implanted and annealed BSO:Si$^+$ samples revealing luminescent peaks centered at 515–520 nm (see Fig. 2) are similar to the PL spectra of SiO_2:Si$^+$ samples reported by other groups.[19–22] For examples, Song *et al.*[19] have shown the PL band centered at about 470 nm for Si$^+$-implanted thermal oxide films with energy of 25 keV and dose of 1×10^{16} cm^{-2} after annealing at < 600°C for 60 min. However, Schuppler *et al.*[23] have observed that the average size of Si nanocrystals responsible for the visible PL is far smaller than 1.3 nm. This corroborates the accuracy of the aforementioned calculation that the PL peak shifts from 780 nm to < 600 nm as the size of Si nanocrystals decreases from 3 nm to < 1.4 nm as previously reported.[24] The improvement of the size of Si nanocrystals (larger than 1 nm) relies strictly on increasing the annealing temperature to 800°C or higher. Nonetheless, most research has attributed the green or yellow PL peaks to the contribution of non-bridging oxygen hole center (NBOHC, O_3 ≡Si–O) or the ≡Si–Si≡ based radiative defects rather than the Si nanocrystals in the Si-implanted SiO_2 samples.[25] In addition, the PL spectra of BSO:Si$^+$ after long-term annealing process do not shift in wavelength but peak intensity decays, which may thus be interpreted as the elimination of the radiative defects. Although few reports have discussed similar phenomenon,[25] it is believed that the *in-situ* annealing process was concurrently initiated with the implantation process, since the BSO glass was also heated during implantation owing to its smaller coefficient of thermal conductivity as compared to that of typical Si substrate. Therefore, the radiative defects in the BSO:Si$^+$ sample have already been activated during the implanting process. Further annealing simultaneously results in the reduction in density of these defects and the precipitation of sub-nm Si nanocrystals. In this case, such a decrease in PL intensity may qualitatively be interpreted as the modification in defect-assistant characteristics of the BSO:Si$^+$ furnace-annealed at 500°C for longer durations.

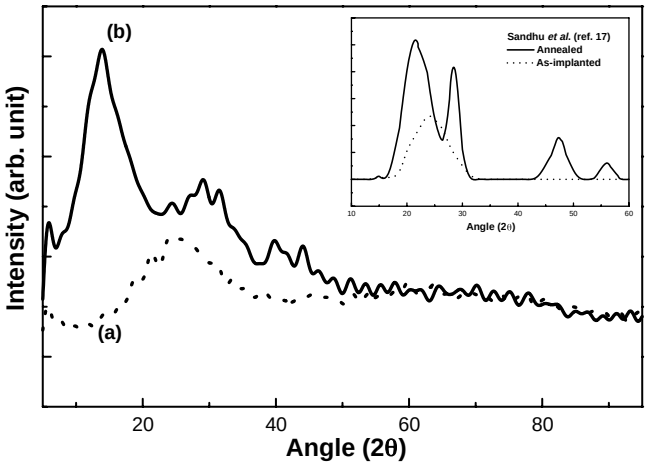

Fig. 1. X-ray diffraction of (a) as-implanted and (b) annealed BSO:Si$^+$ samples. The inset shows the results of silicon-doped BSO film grown on (100) silicon substrate for comparison.

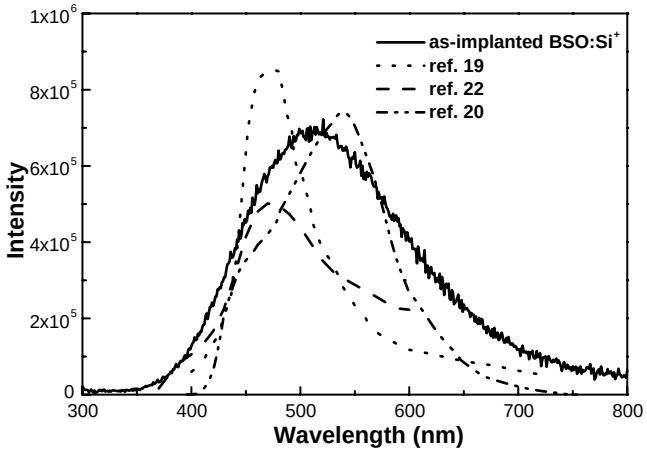

Fig. 2. Photoluminscence spectra of as-implanted BSO:Si$^+$ substrate (solid line) and as-implanted SiO_2:Si$^+$ on silicon substrate (dotted, dashed, and dash-dot-dot lines) measured by different research groups.

To characterize the electrical properties of the BSO:Si^+ material, the leakage current of the Shottky diodes with TLM patterns (referred to as TLM diodes) of different spacings made on the BSO:Si^+ and non-implanted BSO glass substrates were measured and plotted as a function of bias voltage, as shown in Fig. 3. It is seen that the TLM diode with spacing of 2.5 μm made on non-implanted BSO glass exhibits nearly insulating property with leakage current of less than 5 pA and breakdown voltage of up to 400 V, as shown in the inset of Fig. 3. As the spacing of the TLM patterns on glass increases up to 25 μm, the leakage current becomes as small as 1 pA (which is another limitation of the system) at bias of larger than 500 V, and the breakdown voltage further increases to 620 V. After implanting with silicon ions, the current–voltage characteristics of the BSO:Si^+ TLM diodes reveal completely different features. For example, the leakage current of the TLM diode with pattern spacing of 2.5 μm made on the as-implanted BSO:Si^+ substrate greatly increases (overshoots) up to 1.5 nA at bias of 80 V, however, it subsequently decays to 0.9 nA at higher biases. In comparison, the current–voltage characteristic of the diode made on glass has a relatively linear relationship at biases before breakdown. Such an overshooting phenomenon in current–voltage characteristics reveals the existence of negative differential resistance (NDR) effect in BSO:Si^+ samples, which is repeatable for TLM diodes with different spacings. Note that the NDR effect has never been observed in samples with glass substrate and is primarily reported for the metal-semiconductor-metal (MSM) diode made on the silicon-implanted (or silicon-rich) BSO glass. In addition, the peak overshooting voltage tends to occur at higher biases for the diode with larger contact spacings. However, the electrodes of the BSO:Si^+ diode with spacing of 2.5 μm eventually breakdown due to instantaneous air discharge as the bias increases to 330 V. The breakdown voltage of the as-implanted BSO:Si^+ diode with contact spacing of 25 μm can be as high as 550 V. The TLM results of as-implanted BSO:Si^+ and BSO glass samples are shown in Fig. 4. It is found that the measured total resistance and contact resistance of the BSO glass substrate significantly decrease by at least 4 and 3 orders of magnitude, respectively, after Si-ion implantation. For the BSO glass sample, we determined

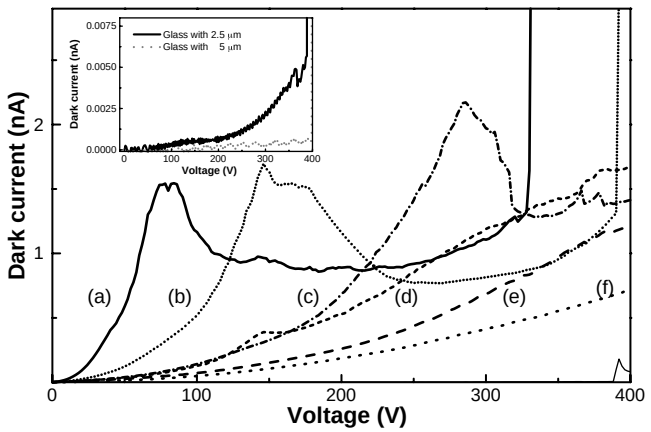

Fig. 3. Measured current–voltage response of TLM diodes with contact spacing of (a) 2.5 μm, (b) 5 μm, (c) 10 μm, (d) 15 μm, (e) 20 μm and (f) 25 μm fabricated on as-implanted BSO:Si^+ substrate.

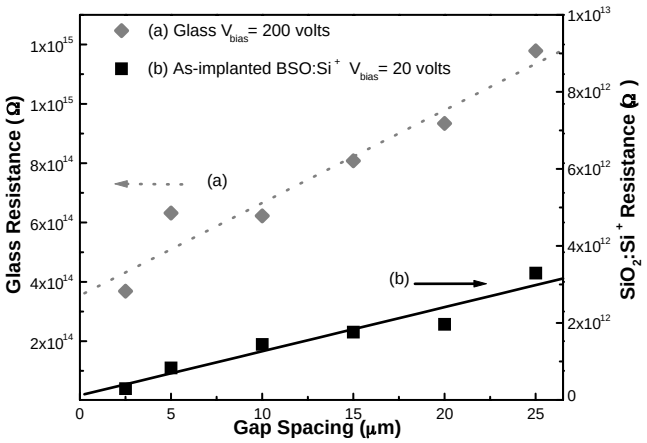

Fig. 4. Measured resistance of TLM diodes made on BSO glass and as-implanted BSO:Si^+ substrates plotted as a function of contact spacing.

the contact and sheet resistances to be about $1.8 \times 10^{14}\,\Omega$ and $2.3 \times 10^{15}\,\Omega/\square$ at 20 V, respectively. After implantation of silicon ions, the contact resistance of the BSO:Si^+ diode abruptly decreases to about $5.9 \times 10^{10}\,\Omega$, and the sheet resistance of BSO:Si^+ also decreases to $8.6 \times 10^{12}\,\Omega/\square$ at 20 V. The specific contact resistivity ρ_c of the BSO glass and as-implanted BSO:Si^+ samples were calculated to be $7.7 \times 10^8\,\Omega\cdot\text{cm}^2$ and $2.3 \times 10^4\,\Omega\cdot\text{cm}^2$, respectively.

In view of these electrical properties, we thus conclude that the electrical property of the BSO glass has been modified from an insulating to a defect-assistant carrier transport process due to the silicon-ion implantation process. The huge leakage current of the BSO:Si^+ diode induced by Si implantation leads to nonlinear, overshooting, and rectified (or resonant tunneling) current–voltage characteristics. On the other hand, the leakage current of the TLM diode made on post-annealed BSO:Si^+ substrate was found to decrease by at least two orders of magnitude compared with that made on as-implanted BSO:Si^+ substrate. The contact or sheet resistance of the TLM diode on BSO:Si^+ substrate is recovered after annealing. The evaluated contact resistance, sheet resistance, specific contact resistivity, and breakdown voltage of the Shottky diodes made on BSO:Si^+ and BSO glass are listed in Table I. Furthermore, the breakdown voltage of the BSO:Si^+ diode increases as the annealing time increases. After annealing at 500°C, the breakdown voltage of BSO:Si^+ TLM diode with 2.5 μm spacing further increases from 354 V to 380 V as annealing time increases from 30 to 120 min, which is close to the value of the same device made on BSO glass. It is thus believed that the carrier transport mechanism of the as-implanted BSO:Si^+ has been degraded due to

Table I. The characteristic parameters of TLM diodes made on different substrates.

Sample	R_c (Ω)	R_s ($\Omega/\square$)	ρ_c ($\Omega\cdot\text{cm}^2$)	$V_{\text{Breakdown}}$
Glass	1.76×10^{14}	2.25×10^{15}	7.744×10^8	390
As-implanted BSO:Si^+	5.9×10^{10}	8.625×10^{12}	2.27×10^4	330
Annealed BSO:Si^+ for 30 min	1.01×10^{14}	1.46×10^{15}	3.93×10^8	354

the elimination of implanted-related defects during long-term thermal annealing. As the annealing time increases to more than 60 min, the leakage current of the BSO:Si^+ is reduced to a value equivalent to or even smaller than that of glass. This could be interpreted as a result of the reduction in density of defects in the BSO:Si^+ after annealing, and thus the contribution of sub-nm Si nanocrystals buried in the BSO:Si^+ sample is negligible.

In conclusion, we have primarily demonstrated the characterization of silicon-ion-implanted BSO glass substrate. Electrical properties such as leakage current and breakdown voltage, as well as other structural characteristics, and the TLM diodes with different Schottky-contact spacings fabricated on the BSO:Si^+ materials have been measured and discussed. The XRD analysis reveals the transformation of a nearly amorphous structure of as-implanted BSO:Si^+ into a slightly crystallite surface associated with two relatively small peaks positioned at $2\theta = 29°$ and 14°, which corresponds to the formation of sub-nm Si nanocrystallite with (111) orientation and recrystallized (021)-oriented SiO_2 phase of BSO. The continuous-wave PL indicate a luminescent peak at about 520 nm ($\sim$ 2.5 eV) under the pumping wavelength of 270 nm ($\sim$ 4.6 eV). The decrease of PL intensity corroborates the elimination of radiative defects in the annealed BSO:Si^+ sample. The significant leakage current of the defect-assistant carrier transport in BSO:Si^+ measured by TLM analysis reveals an overshooting and rectified characteristic for the BSO:Si^+ diode. The overshooting voltage increases as the gap spacing between contacts of TLM diodes increases, however, it diminishes after long-term annealing. This suggests that the effect of defects on the resonant tunneling behavior of the BSO:Si^+ diode is more pronounced than that of Si nanocrystals. The leakage current of the TLM diode made on annealed BSO:Si^+ substrate is further decreased by at least two orders of magnitude more than that made on as-implanted substrate. The current–voltage and breakdown analysis confirm the disappearance of the negative differential resistance property in BSO:Si^+ after annealing at 500°C for longer than 60 min.

This work was supported in part by the National Science Council (NSC) of the Republic of China under grants NSC 89-2215-E-027-007 and NSC 90-2215-E-027-008. Technical support of this work by the Optical Science Center at National Central University is also appreciated. The author thanks Mr. Chin-Chia Hsu for obtaining most of the experimental data.

1) A. G. Cullis, L. T. Canham and P. D. Calcott: J. Appl. Phys. **82** (1997) 909.
2) V. Lehmann and U. Gosele: Appl. Phys. Lett. **58** (1991) 856.
3) D. J. DiMaria, J. R. Kirtley, E. J. Pakulis, D. W. Dong, T. S. Kuan, F. L. Pesavento, T. N. Theis and J. A. Cutro: J. Appl. Phys. **56** (1984) 401.
4) S. Furukawa and T. Miyasato: Jpn. J. Appl. Phys. **27** (1988) 2207.
5) H. Takagi, H. Ogawa, Y. Yamazaki and T. Nakagiri: Appl. Phys. Lett. **56** (1990) 2379.
6) H. Morisaki, F. W. Ping, H. Ono and K. Yazawa: J. Appl. Phys. **70** (1991) 1869.
7) S. Hayashi, T. Nagareda, Y. Kanzawa and K. Yamamoto: Jpn. J. Appl. Phys. **32** (1993) 3840.
8) L. T. Canham: Appl. Phys. Lett. **57** (1990) 1046.
9) *Materials and Devices for Silicon-Based Optoelectronics*, eds. S. Coffa, A. Polman and O. Soref (Material Research Society, Pittsburgh, 1998) Mater. Res. Soc. Symp. Proc. Vol. 486.
10) C. Delerue, G. Allan and M. Lannoo: Phys. Rev. B**48** (1993) 11024.
11) K. S. Min, K. V. Shchegloe, C. M. Yang, H. A. Atwater, M. L. Brongersma and A. Polman: Appl. Phys. Lett. **69** (1996) 2033.
12) S. Tiwari, F. Rana, H. Hanafi, A. Hartstein, E. Crabbe and K. Chan: Appl. Phys. Lett. **68** (1996) 1377.
13) K. D. Hirschman, L. Tsybeskov, S. D. Duttagupta and P. M. Fauchet: Nature (London) **384** (1996) 338.
14) Y. Kanemitsu: Phys. Rep. **263** (1995) 1.
15) M. L. Brongersma, K. S. Min, E. Boer, T. Tambo, A. Polman and H. A. Atwater: Mater. Res. Soc. Symp. Proc. **486** (1998) 275.
16) L. Rebohle, J. von Borany, R. A. Yankov, W. Skorupa, I. E. Tyscenko, H. Fröb and K. Leo: Appl. Phys. Lett. **71** (1997) 2809.
17) A. Sandhu, Y. Show, T. Katano, M. Iwase, T. Izumi, T. Yabe, S. Nozaki and H. Morisaki: Appl. Sur. Sci. **117** (1997) 634.
18) See for example, JCPDS-International Center for Diffraction Data, No. 35–63, **82** (1999) Newtown Square, Pennsylvania 19073-3273 U.S.A.
19) H. Z. Song, X. M. Bao, N. S. Li and J. Y. Zhang: J. Appl. Phys. **82** (1997) 4028.
20) L. S. Liao, X. M. Bao, N. S. Li, X. Q. Zheng and N. B. Min: J. Lumin. **68** (1996) 199.
21) P. Mutti, G. Ghislotti, L. Meda, E. Grilli, M. Guzzi, L. Zanghieri, R. Cubeddu, A. Pifferi, P. Taroni and A. Torricelli: Thin Solid Films **276** (1996) 88.
22) L. Rebohle, I. E. Tyschenko, H. Frob, K. Leo, R. A. Yankov, J. von Borany, G. A. Kachurin and W. Skorupa: Microelectron. Eng. **36** (1997) 107.
23) S. Schuppler, S. L. Friedman, M. A. Marcus, D. L. Adler, Y.-H. Xie, F. M. Ross, Y. J. Chabal, T. D. Harris, L. E. Brus, W. L. Brown, E. E. Chaban, P. F. Szajowski, S. B. Christman and P. H. Citrin: Phys. Rev. B**52** (1995) 4910.
24) R. K. Soni, L. F. Fonseca, O. Resto, M. Buzaianu and S. Z. Weisz: J. Lumin. **83/84** (1999) 187.
25) J. Y. Jeong, S. Im, M. S. Oh, H. B. Kim, K. H. Chae, C. N. Whang and J. H. Song: Jpn. J. Appl. Phys. **37** (1998) 6981.